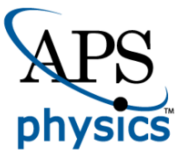

Strong and tunable interlayer coupling of infrared-active phonons to excitons in van der Waals heterostructures

Luojun Du, Yanchong Zhao, Zhiyan Jia, Mengzhou Liao, Qinqin Wang, Xiangdong Guo, Zhiwen Shi, Rong Yang, Kenji Watanabe, Takashi Taniguchi, Jianyong Xiang, Dongxia Shi, Qing Dai, Zhipei Sun, and Guangyu Zhang

Phys. Rev. B **99**, 205410 — Published 10 May 2019

DOI: 10.1103/PhysRevB.99.205410

Strong and tunable interlayer coupling of infrared active phonon to exciton in van der Waals heterostructures

Luojun Du[1,2†]*, Yanchong Zhao[1†], Zhiyan Jia[3], Mengzhou Liao[1], Qinqin Wang[1], Xiangdong Guo[4], Zhiwen Shi[5], Rong Yang[1], Kenji Watanabe[6], Takashi Taniguchi[6], Jianyong Xiang[3], Dongxia Shi[1,7,8], Qing Dai[4], Zhipei Sun[2,10], Guangyu Zhang[1,7,8,9]*

[1]Beijing Key Laboratory for Nanomaterials and Nanodevices, Institute of Physics, Chinese Academy of Sciences, Beijing 100190, China

[2]Department of Electronics and Nanoengineering, Aalto University, Tietotie 3, FI-02150, Finland

[3]State Key Laboratory for Metastable Materials Science and Technology, Yanshan University, Qinhuangdao 066004, China

[4]National Center for Nanoscience and Technology, Beijing 100190, China

[5]Key Laboratory of Artificial Structures and Quantum Control (Ministry of Education), School of Physics and Astronomy, Shanghai Jiao Tong University, Shanghai, China

[6]National Institute for Materials Science, 1-1 Namiki, Tsukuba 305-0044, Japan

[7]School of Physical Sciences, University of Chinese Academy of Science, Beijing 100190, China

[8]Songshan-Lake Materials Laboratory, Dongguan, Guangdong Province, 523808, China

[9]Collaborative Innovation Center of Quantum Matter, Beijing 100190, China

[10]QTF Centre of Excellence, Department of Applied Physics, Aalto University, FI-00076 Aalto, Finland

[†]These authors contributed equally to this work

*Corresponding authors: luojun.du@aalto.fi; gyzhang@aphy.iphy.ac.cn

Understanding and manipulating the quantum interlayer exciton-phonon coupling in van der Waals heterostructures, especially for infrared active phonons with electromagnetic fields, would set a foundation for realizing exotic quantum phenomena and novel optoelectronic applications. Here we report the first experimental observations of strong mutual interactions between infrared active phonons in hBN and excitons in WS_2. Our results underscore that the infrared active A_{2u} mode of hBN becomes Raman active with strong intensities in WS_2/hBN heterostructures through resonant coupling to the B exciton of WS_2. Moreover, we demonstrate that the activated A_{2u} phonon of hBN can be tuned by the

hBN thickness and harbours a striking anticorrelation intensity modulation, as compared with the optically silent B_{1g} mode. Our observation of the interlayer exciton-infrared active phonon interactions and their evolution with hBN thickness provide a firm basis for engineering the hyperbolic exciton–phonon polaritons, chiral phonons and fascinating nanophotonics based on van der Waals heterostructures.

I. INTRODUCTION

Van der Waals (vdW) heterostructures stacked from atomically thin two-dimensional (2D) crystals provide a new paradigm for a cornucopia of intriguing physics and novel device applications [1-5]. Hexagonal boron nitride (hBN), a representative vdW crystal, plays a prominent role in assembling vdW heterostructures. To name but a few, hBN gives rise to the breakthrough for the first vdW heterostructures [1, 6], acts as a perfect substrate for high mobility devices [6-8], and leads to moiré superlattices in graphene/hBN heterostructures [9-11]. More importantly, hBN is a naturally polar and hyperbolic crystal, possessing exotic infrared active phonons and phonon polaritons [12-17]. The infrared active phonon polaritons exhibit high-quality factors and can be localized at sub-diffractional length scales, opening up opportunities for nanophotonics [13, 18]. However, the control of infrared active phonon polaritons has remained challenging, impeding strongly their practical applications [19]. Therefore, it is highly desirable and potentially important to combine the fascinating infrared phonons in hBN with other quasiparticles, offering an unprecedented platform to realize tunable hyperbolic polaritons. Recently, hybridizations of infrared active phonons or hyperbolic phonon polaritons in hBN with electrons in graphene have been uncovered and create new tunable hyperbolic plasmon-phonon polaritons [19-24].

Transition metal dichalcogenides (TMDCs), another elemental building block for vdW heterostructures, harbour extraordinary exciton properties, such as valley selection rules [25-28], electrical control of Coulomb-bound many-body states [29-31] and robust exciton polaritons [32-35]. In principle, excitons in TMDCs would couple to exotic infrared active phonons or hyperbolic phonon polaritons in hBN, enabling another completely new way to generate tunable hyperbolic polaritons [16, 17]. Recently, interlayer exciton-phonon coupling (EPC) associated with optically silent B_{1g} phonons in hBN and excitons in TMDCs has been revealed in WSe_2/hBN [36-38] and $WS_{0.6}Se_{1.4}$/hBN [39] heterostructures, making the optically silent hBN vibration

become Raman active and giving rise to a new electronic transition. However, quantum layer-layer interactions between excitons in TMDCs and infrared active phonons in hBN have remained elusive. Understanding such interlayer exciton-infrared active phonon coupling in TMDCs/hBN heterostructures could be of greater relative importance than the interlayer EPC associated with optically silent B_{1g} modes and provide a firm basis for engineering the tunable hyperbolic exciton-phonon polaritons [12-14, 16, 17].

In this paper, we identify, for the first time, the interlayer coupling between infrared active A_{2u} phonons and excitons in WS_2/hBN vdW heterostructures at room temperature. Moreover, our experiments reveal that the interlayer EPC between the excitons in WS_2 and infrared active A_{2u} phonons in hBN is strongly dependent on the hBN thickness. For WS_2/few-layer hBN heterostructures, the intensities of infrared active A_{2u} phonons drop sharply with a descent of the hBN thickness, in stark contrast to the B_{1g} modes that show a weak increase.

II. SAMPLE PREPARATION AND CHARACTERIZATION

WS_2/hBN heterostructures were obtained via a combination of chemical vapor deposition (CVD) growth and dry transfer. High quality monolayer triangular WS_2 (~ 100 μm) were first grown on 300 nm SiO_2/Si substrates through a CVD process [40]. Atomically thin WS_2 layers were first visually identified by their interference color under the optical microscope and then confirmed by the out-of-plane $A_{1g}(\Gamma)$ mode under excitation on resonance with A exciton (see Supplemental Material [41]). A polydimethylsiloxane (PDMS) stamp was then used to place hBN flakes on monolayer WS_2 in a vacuum chamber, forming the WS_2/hBN heterostructures. This vacuum transfer method greatly improves the interface quality and minimizes the amount of amorphous carbon or trapped air at the interfaces [42]. The heterostructures were then annealed at 280°C in an Ar/H_2 atmosphere to further clean the interface and improve the layer-layer interactions. Figure 1(a) presents an optical microscope image of the WS_2/hBN heterostructures highlighted by red lines. The height image obtained from a tapping mode atomic force microscopy (AFM) scanning of the square region in Fig. 1(a) is presented in Fig. 1(b). The flat morphology of the heterostructures display very low root-mean-square (RMS) surface roughness of 0.42 nm (see Supplemental Material [41]), demonstrating that the WS_2/hBN heterostructures obtained via vacuum transfer can possess very larger clean and smooth regions (lateral size > 15 μm) devoid of

bubbles. The height line scan profile indicates that the thickness of hBN is 3.6 nm. The photoluminescence (PL) spectra of WS_2 and WS_2/hBN heterostructures are shown in Fig. 1(c). Both the WS_2 and WS_2/hBN heterostructures harbour a single narrow A exciton feature centered at 1.963 eV, indicating the direct-gap of monolayer WS_2 [40, 43]. Strikingly, we can see a prominent difference between WS_2 and WS_2/hBN heterostructures. Compared with WS_2, the PL intensity of WS_2/hBN heterostructures is doubled and the full width at half maximum (FWHM) decreases from 42 meV to 34 meV. Such enhanced PL intensity and reduction of FWHM stem from the effective suppression of inhomogeneous contribution via surface protection [44, 45]. Figure 1(d) presents the Raman spectra of WS_2 and WS_2/hBN heterostructures excited by 2.33 eV radiation. It can be seen that the Raman spectrum of WS_2/hBN heterostructures is almost the same as that of WS_2. In contrast to MoS_2 that possesses only two prominent Raman modes ($E^1_{2g}(\Gamma)$ and $A_{1g}(\Gamma)$) under 532 nm excitation [46-48], we can observe not only the $A_{1g}(\Gamma)$ and $E^1_{2g}(\Gamma)$ modes, but also a series of multiple phonon replica, combination and edge phonons of the hexagonal Brillouin zone in WS_2 (see Supplemental Material [41]), stemming from that the excitation energy 2.33 eV is on resonance with the B exciton of WS_2 [40, 49].

III. RESULTS AND DISCUSSION

Since interlayer EPC is a defining feature of resonant Raman scattering [36, 37], the giant PL background from A exciton of monolayer TMDCs brings much inconvenience to measure the interlayer EPC. To derive the interlayer EPC of WS_2/hBN heterostructures at room temperature, the hindrance of PL background is more pronounced since PL quantum efficiency is very huge (~ 1200 times larger than that of MoS_2 [Fig. 2(a)]) and much larger than that at cryogenic temperature due to dark excitons with lower energy [50-52]. There are two ways to avoid the PL background. First, if WS_2/hBN heterostructures have null valley coherence, we can derive the interlayer EPC without the PL background by subtracting the cross-polarization spectra from the parallel-polarization spectra, provided that the Raman excitations are suppressed in cross-polarized geometry [36]. However, our WS_2/hBN heterostructures possess robust valley coherence at room temperature [Fig. 2(b)], thus we cannot obtain the interlayer EPC without PL background in this method via using excitation, on resonance with the A exciton of WS_2. Another way is that we can use the laser radiation on resonance with the other excitons, such as B and A′ excitons, since the intensity of these excitons are much weaker than that of A exciton. In fact,

clear signals associated with interlayer EPC have been uncovered in WSe_2/hBN heterostructures via resonant coupling to the A′ exciton of WSe_2 [37, 38]. In this paper, we take advantage of the B exciton to obtain clear Raman features about interlayer EPC without the PL background.

Figure 3(c) presents the Raman spectra of hBN, WS_2 and WS_2/hBN heterostructures excited by 2.33 eV excitation, on resonance with the B exciton of WS_2 [49]. Compared with the Raman spectra of hBN and WS_2, two new Raman signals around 800 cm^{-1} emerge in WS_2/hBN heterostructures, indicated by the dashed black vertical lines. Through Lorentzian fitting [Fig. 3(d)], it is prone to know that these two new Raman modes locate at 767 and 803 cm^{-1}, respectively, which should be Raman forbidden hBN phonons activated in WS_2/hBN heterostructures via interlayer EPC [36, 37, 39]. In addition, the intensities of the Raman forbidden hBN phonons are stronger than that of the Raman active E_{2g} phonon at 1367 cm^{-1}. This clearly indicates the strong interlayer EPC.

The crystal structure of lamellar hBN belongs to the D_{6h}^4 ($P6_3/mmc$) space group. According to group theory, the corresponding irreducible representations of phonons at the Brillouin-zone center can be divided into: $\Gamma = 2E_{1u} + 2E_{2g} + 2A_{2u} + 2B_{1g}$ [53-55]. Only the E_{2g} phonon, involving in-plane atomic displacements in the hexagonal layers, is Raman active at 1367 cm^{-1}. For the infrared active A_{2u} mode [Fig. 3(a)], the crystal field in hBN gives rise to a splitting between transverse (TO) and longitudinal (LO) optical phonons, located at 767 cm^{-1} and 825 cm^{-1}, respectively [55]. Due to the presence of electromagnetic fields for the TO mode, it can be strongly coupled with other quasiparticles, such as photon, the electron and plasmon polaritons [19-24]. From Fig. 3(d), it can be clearly seen that the active Raman mode with lower energy is at 767 cm^{-1}, matching well with the TO mode of infrared active A_{2u} phonon. While, for the active Raman mode with higher energy [Fig. 3(d)], it cannot be assigned to the LO mode of A_{2u} since the phonon frequency (803 cm^{-1}) is obvious different from the LO mode (825 cm^{-1}). It makes sense that the excitons in WS_2 do not couple to the LO mode in hBN since the LO mode is accompanied by only an electric field without curl (being akin to an electrostatic field) [56]. In addition, according to theoretical calculations [53], there is another phonon, optically silent B_{1g} [Fig. 3(b)], located around 809 cm^{-1}. Despite a little difference, B_{1g} mode shows qualitative agreement with the active Raman mode with higher energy [Fig. 3(d)]. Recently, Raman forbidden phonons in hBN have been found to be activated in WSe_2/hBN heterostructures and locate at 806 cm^{-1} and

798 cm^{-1} for refs. 36 and 37, respectively [57]. We believe that such activated modes in WSe_2/hBN heterostructures should be the phonon with higher energy in Fig. 3(d) (B_{1g} mode) since it is quite distinct from both the TO and LO modes of infrared active A_{2u} phonons. The differences between different experimental results may stem from distinct hBN thickness, as will be discussed below. Thus, our results demonstrate, for the first time, the interlayer coupling between the infrared active A_{2u} phonons of hBN and the excitons of WS_2, which will shed light on the engineering of hyperbolic exciton–phonon polaritons and chiral phonons [16, 17, 58-60]. Figure 3e shows the power-dependent Raman spectra of another WS_2/hBN heterostructures sample with similar hBN thickness. The Raman intensities increase with the incident power. Figure 3f shows the power dependent Raman intensity ratio between the infrared active A_{2u} (and optically silent B_{1g}) phonon and Raman active E_{2g} phonon at 1367 cm^{-1}. It shows that the Raman intensity ratio between the infrared active A_{2u} (optically silent B_{1g}) phonon and Raman active E_{2g} phonon is ~ 2.7 (1.5) and independent on the incident light power. In addition, we observe a new Raman peak located at 1125 cm^{-1} for WS_2 and WS_2/hBN heterostructures (Fig. 2(c) and Fig. 4). However, this new Raman mode cannot be observed in pristine hBN on SiO_2 or WS_2 grown on sapphire (Fig. 2(c) and Fig. 4). Therefore, this new Raman mode at 1125 cm^{-1} in WS_2 and WS_2/hBN heterostructures should be the surface phonon mode of SiO_2, which resonantly couples to B exciton of WS_2 [12, 37, 60, 61].

Having demystified the interlayer EPC in WS_2/hBN heterostructures, we carried out the polarization-resolved Raman spectra to confirm the symmetry of the activated A_{2u} and B_{1g} phonons. Figure 5(a) presents the Raman spectra under co-polarization configuration and cross-polarization configuration. It shows that the intensities of both the activated A_{2u} and B_{1g} phonons depend strongly on the polarization configurations and almost disappear in cross-polarization configuration. Figure 5(b) shows the normalized Raman intensity of A_{2u} and B_{1g} modes as a function of angle θ between e_i and e_s. The normalized intensities of both A_{2u} and B_{1g} phonons harbour the same periodical oscillation and can be fitted well with a cosine function ($\cos^2\theta$), indicating that A_{2u} and B_{1g} phonons possess the same symmetry. The same symmetry is due to that the interlayer coupling between WS_2 and hBN lowers the symmetry of the WS_2/hBN heterostructures and both the original A_{2u} and B_{1g} modes of hBN become an A mode [36].

Naturally, the dimensionality of a system has profound impacts on both phonons and excitons

[38, 62-64]. To elaborate the influence of hBN thickness on interlayer EPC of WS_2/hBN heterostructures, we covered a thin hBN with various thicknesses on monolayer WS_2 by a dry transfer method. Figure 6(a) presents the microscopic image of WS_2/hBN heterostructures with different thickness of hBN. To rule out extrinsic factors, we focus on such WS_2/hBN heterostructures with distinct hBN thicknesses, but fixed twisting angle between hBN and WS_2 and interfacial coupling [65-69]. Figure 6(b) shows the corresponding Raman spectra. It shows that the intensities of activated phonons in WS_2/hBN heterostructures strongly depend on the hBN thickness. Figure 6(c) displays the integrated intensities of the infrared active A_{2u} and optically silent B_{1g} phonons in WS_2/hBN heterostructures as a function of hBN thickness. With increasing the hBN thickness, the intensities of infrared active A_{2u} mode are enhanced significantly, while the intensities of B_{1g} mode decline slowly. Such hBN thickness-driven anticorrelation intensity modulation between A_{2u} and B_{1g} phonons is fairly amazing since A_{2u} and B_{1g} modes show similar polarization behavior (Fig. 5). Because the interlayer EPC is associated with the out-of-plane electric dipole of a phonon [37], the physical origin for the hBN thickness-induced anticorrelation intensity modulation may stem from the different electric dipole between the A_{2u} and B_{1g} modes. For the B_{1g} mode, there is an in-phase combination between adjacent layers and therefore, it only has an intralayer electric dipole [Fig. 6(f)]. Because the excitons in WS_2 are strongly confined to the 2D plane [70, 71], the interlayer EPC in WS_2/hBN heterostructures is dominated by the phonons of hBN in the immediate vicinity of WS_2. Such layer-layer interaction should decrease with increasing the hBN thickness and disappear for bulk hBN [36, 37]. This is in good harmony with our results that the intensities of B_{1g} mode decline with increasing hBN thickness and are absent in WS_2/bulk hBN heterostructures (see Supplemental Material [41]). In stark contrast, infrared active A_{2u} mode is a lattice vibration with antiphase displacement in adjacent layers and can possess not only an intralayer electric dipole, but also an interlayer electric dipole [Fig. 6(e)]. The interlayer electric dipole can extend the interlayer EPC to a large volume of phonons spread throughout the hBN that do not interact directly with WS_2. Due to volume effect, the intensities of infrared active A_{2u} modes in WS_2/few-layer hBN heterostructures can increase with increasing the hBN thickness. In addition to the tunable strength of interlayer EPC, the energy of activated phonons can be also tuned via hBN thickness. Figure 6(d) shows the hBN thickness dependent phonon energies of the activated A_{2u} and B_{1g} phonons in WS_2/hBN heterostructures. With

increasing the hBN thickness, the infrared active A_{2u} phonon softens, while the B_{1g} mode stiffens. The evolution of phonon energies with hBN thickness may be the reason for the small difference of B_{1g} phonon frequency between our results [Fig. 3(d)] and the results in refs. 36 and 37.

IV. CONCLUSIONS

In conclusion, we have measured interlayer EPC of WS_2/hBN heterostructures through resonant coupling to the B exciton of WS_2 at room temperature. We demonstrate for the first time that the infrared active A_{2u} phonons in hBN can strongly couple to the excitons in WS_2. Moreover, our results demonstrate that the strength of interlayer EPC can be tuned by hBN thickness. The strength of interlayer EPC associated with infrared active A_{2u} phonon is almost zero for monolayer hBN and increases sharply with increasing the hBN thickness, in stark contrast to the B_{1g} mode that harbours a weak decrease. In addition, we uncover that the energies of activated phonons could be also tuned by hBN thickness. We believe that our observation of the strong and tunable interlayer coupling between infrared active phonons and excitons will shed light on the manipulation of new hybrid quasiparticles and polaritons, and engineering of novel optoelectronic applications based on vdW heterostructures.

Acknowledgment

We acknowledge the comments and suggestions raised by Prof. Tobias Korn from University of Rostock and Luke Baker from Aalto University. This work was supported by the National Science Foundation of China (NSFC, Grant Nos. 61734001, 11834017 and51572289), the Strategic Priority Research Program (B) of CAS (Grant No. XDB30000000), the National Key R&D program of China (Grant No. 2016YFA0300904), the Key Research Program of Frontier Sciences of CAS (GrantNo. QYZDB-SSW-SLH004) and the Youth InnovationPromotion Association of CAS (No. 2018013). Growth of hexagonal boron nitride crystals was supported by the Elemental Strategy Initiative conducted by the MEXT, Japan and the CREST (JPMJCR15F3), JST.

[1] A. K. Geim and I. V. Grigorieva, Nature **499**, 419 (2013).

[2] K. Novoselov, A. Mishchenko, A. Carvalho, and A. C. Neto, Science **353**, aac9439 (2016).

[3] Y. Liu, N. O. Weiss, X. Duan, H.-C. Cheng, Y. Huang, and X. Duan, Nat. Rev. Mater. **1**, 16042 (2016).

[4] J. R. Schaibley, P. Rivera, H. Yu, K. L. Seyler, J. Yan, D. G. Mandrus, T. Taniguchi, K. Watanabe, W. Yao, and X. Xu, Nat. Commun. **7**, 13747 (2016).

[5] S. Manzeli, D. Ovchinnikov, D. Pasquier, O. V. Yazyev, and A. Kis, Nat. Rev. Mater. **2**, 17033 (2017).

[6] C. R. Dean, A. F. Young, I. Meric, C. Lee, L. Wang, S. Sorgenfrei, K. Watanabe, T. Taniguchi, P. Kim, K. L. Shepard, and J. Hone, Nat. Nanotechnol. **5**, 722 (2010).

[7] X. Cui, G.-H. Lee, Y. D. Kim, G. Arefe, P. Y. Huang, C.-H. Lee, D. A. Chenet, X. Zhang, L. Wang, F. Ye, F. Pizzocchero, B. S. Jessen, K. Watanabe, T. Taniguchi, D. A. Muller, T. Low, P. Kim, and J. Hone, Nat. Nanotechnol. **10**, 534 (2015).

[8] L. Li, F. Yang, G. J. Ye, Z. Zhang, Z. Zhu, W. Lou, X. Zhou, L. Li, K. Watanabe, T.Taniguchi, K. Chang, Y. Wang, X.Chen, and Y. Zhang, Nat. Nanotechnol. **11**, 593 (2016).

[9] B. Hunt, J. D. Sanchez-Yamagishi, A. F. Young, M. Yankowitz, B. J. LeRoy, K. Watanabe, T. Taniguchi, P. Moon, M. Koshino, P. Jarillo-Herrero, and R. C. Ashoori, Science **340**, 1427 (2013).

[10] C. Dean, L. Wang, P. Maher, C. Forsythe, F. Ghahari, Y. Gao, J. Katoch, M. Ishigami, P. Moon, M. Koshino, T. Taniguchi, K. Watanabe, K. L. Shepard, J. Hone, and P. Kim, Nature **497**, 598 (2013).

[11] W. Yang, G. Chen, Z. Shi, C.-C. Liu, L. Zhang, G. Xie, M. Cheng, D. Wang, R. Yang, D. Shi, K.Watanabe, T. Taniguchi, Y. Yao, Y. Zhang, and G. Zhang, Nat. Mater. **12**, 792 (2013).

[12] S. Dai, Z. Fei, Q. Ma, A. S. Rodin, M. Wagner, A. S. McLeod, M. K. Liu, W. Gannett, W. Regan, K. Watanabe, T. Taniguchi, M. Thiemens, G. Dominguez, A. H. Castro Neto, A. Zettl, F. Keilmann, P. Jarillo-Herrero, M. M. Fogler, and D. N. Basov, Science **343**, 1125 (2014).

[13] J. D. Caldwell, A. V. Kretinin, Y. Chen, V. Giannini, M. M. Fogler, Y. Francescato, C. T. Ellis, J. G. Tischler, C. R. Woods, A. J. Giles, M. Hong, K. Watanabe, T. Taniguchi, S. A. Maier, and K. S. Novoselov, Nat. Commun. **5**, 5221 (2014).

[14] Z. Shi, H. A. Bechtel, S. Berweger, Y. Sun, B. Zeng, C. Jin, H. Chang, M. C. Martin, M. B. Raschke, and F. Wang, ACS Photonics **2**, 790 (2015).

[15] E. Yoxall, M. Schnell, A. Y. Nikitin, O. Txoperena, A. Woessner, M. B. Lundeberg, F. Casanova, L. E. Hueso, F. H. L. Koppens, and R. Hillenbrand, Nat. Photonics **9**, 674 (2015).

[16] D. Basov, M. Fogler, and F. G. de Abajo, Science **354**, aag1992 (2016).

[17] T. Low, A. Chaves, J. D. Caldwell, A. Kumar, N. X. Fang, P. Avouris, T. F. Heinz, F. Guinea,

L. Martin-Moreno, and F. Koppens, Nat. Mater. **16**, 182 (2017).

[18] S. Dai, Q. Ma, T. Andersen, A. S. Mcleod, Z. Fei, M. K. Liu, M. Wagner, K. Watanabe, T. Taniguchi, M. Thiemens, F. Keilmann, P. Jarillo-Herrero, M. M. Fogler, and D. N. Basov, Nat. Commun. **6**, 6963 (2015).

[19] S. Dai, Q. Ma, M. K. Liu, T. Andersen, Z. Fei, M. D. Goldflam, M. Wagner, K. Watanabe, T. Taniguchi, M. Thiemens, F. Keilmann, G. C. A. M. Janssen, S-E. Zhu, P. Jarillo-Herrero, M. M. Fogler, and D. N. Basov, Nat. Nanotechnol. **10**, 682 (2015).

[20] V. W. Brar, M. S. Jang, M. Sherrott, S. Kim, J. J. Lopez, L. B. Kim, M. Choi, and H. Atwater, Nano Lett. **14**, 3876 (2014).

[21] X. Yang, F. Zhai, H. Hu, D. Hu, R. Liu, S. Zhang, M. Su, Z. Sun, J. Chen, and Q. Dai, Adv. Mater. **28**, 2931 (2016).

[22] A. Kumar, T. Low, K. H. Fung, P. Avouris, and N. X. Fang, Nano Lett. **15**, 3172 (2015).

[23] K.-J. Tielrooij, N. C. H. Hesp, A. Principi, M. B. Lundeberg, E. A. A. Pogna, L.Banszerus, Z. Mics, M. Massicotte, P. Schmidt, D. Davydovskaya, D. G. Purdie, I. Goykhman, G. Soavi, A. Lombardo, K. Watanabe, T. Taniguchi, M. Bonn, D. Turchinovich, C. Stampfer, A. C. Ferrari, G. Cerullo, M. Polini, and F. H. L. Koppens, Nat. Nanotechnol. **13**, 41 (2018).

[24] W. Yang, S. Berthou, X. Lu, Q. Wilmart, A. Denis, M. Rosticher, T. Taniguchi, K. Watanabe, G. Fève, J.-M. Berroir, G. Zhang, C. Voisin, E. Baudin, and B. Plaçais, Nat. Nanotechnol. **13**, 47 (2018).

[25] K. F. Mak, K. He, J. Shan, and T. F. Heinz, Nat. Nanotechnol. **7**, 494 (2012).

[26] H. Zeng, J. Dai, W. Yao, D. Xiao, and X. Cui, Nanotechnol. **7**, 490 (2012).

[27] A. M. Jones, H.Yu, N. J. Ghimire, S. Wu, G. Aivazian, J. S. Ross, B. Zhao, J. Yan, D. G. Mandrus, D. Xiao, W. Yao, and X. Xu, Nat. Nanotechnol. **8**, 634 (2013).

[28] R. Schmidt, A. Arora, G. Plechinger, P. Nagler, A. G. del Águila, M. V. Ballottin, P. C. M. Christianen, S. M. de Vasconcellos, C. Schüller, T. Korn, and R. Bratschitsch, Phys. Rev. Lett. **117**, 077402 (2016).

[29] K. F. Mak, K. He, C. Lee, G. H. Lee, J. Hone, T. F. Heinz, and J. Shan, Nat. Mater. **12**, 207 (2012).

[30] J. S. Ross, S. Wu, H. Yu, N. J. Ghimire, A. M. Jones, G. Aivazian, J. Yan, D. G. Mandrus, D. Xiao, W. Yao, and X. Xu, Nat. Commun. **4**, 1474 (2013).

[31] P. Nagler, M. V. Ballottin, A. A. Mitioglu, M. V. Durnev, T.Taniguchi, K. Watanabe, A. Chernikov, C. Schüller, M. M. Glazov, P. C. M. Christianen, and T. Korn, Phys. Rev. Lett. **121**, 057402 (2018).

[32] X. Liu, T. Galfsky, Z. Sun, F. Xia, E.-c. Lin, Y.-H. Lee, S. Kéna-Cohen, and V. M. Menon, Nat. Photonics **9**, 30 (2015).

[33] F. Hu, Y. Luan, M. Scott, J. Yan, D. Mandrus, X. Xu, and Z. Fei, Nat. Photonics **11**, 356 (2017).

[34] Z. Fei, M. E. Scott, D. J. Gosztola, J. J. Foley, IV, J. Yan, D. G. Mandrus, H. Wen, P. Zhou, D. W. Zhang, Y. Sun, J. R. Guest, S. K. Gray, W. Bao, G. P. Wiederrecht, and X. Xu, Phys. Rev. B **94**, 081402 (2016).

[35] N. Lundt, S. Klembt, E. Cherotchenko, S. Betzold, O. Iff, A. V. Nalitov, M. Klaas, C. P. Dietrich, A. V. Kavokin, S. Höfling, and C. Schneider, Nat. Commun.**7**, 13328 (2016).

[36] C. Jin, J. Kim, J. Suh, Z. Shi, B. Chen, X. Fan, M. Kam, K. Watanabe, T. Taniguchi, S. Tongay, A. Zettl, J. Wu, and F. Wang, Nat. Phys. **13**, 127 (2017).

[37] C. M. Chow, H. Yu, A. M. Jones, J. Yan, D. G. Mandrus, T. Taniguchi, K. Watanabe, W. Yao, and X. Xu, Nano Lett. **17**, 1194 (2017).

[38] L. Du, M. Liao, J. Tang, Q. Zhang, H. Yu, R. Yang, K.Watanabe, T. Taniguchi, D. Shi, Q. Zhang, and G. Zhang, Phys. Rev. B **97**, 235145 (2018).

[39] Y. Meng, T. Wang, Z. Li, Y. Qin, Z. Lian, Y. Chen, M. C. Lucking, K. Beach, T. Taniguchi, K. Watanabe, S. Tongay, F. Song, H. Terrones, and S.-F. Shi, Nano Lett. **19**, 299 (2019).

[40] L. Du, Z. Jia, Q. Zhang, A. Zhang, T. Zhang, R. He, R. Yang, D. Shi, Y. Yao, J. Xiang, G. Zhang, and Qingming Zhang, 2D Mater. 5, 035028 (2018).

[41] See Supplemental Material for details on resonant Raman, Raman Peak assignments, RMS surface roughness, and WS_2/hBN heterostructures with bulk hBN.

[42] K. Kang, K.-H. Lee, Y. Han, H. Gao, S. Xie, D. A. Muller, and J. Park, Nature **550**, 229 (2017).

[43] H. Zeng, G.-B. Liu, J. Dai, Y. Yan, B. Zhu, R. He, L. Xie, S. Xu, X. Chen, W. Yao, and X. Cui, Sci. Rep. **3**, 1608 (2013).

[44] F. Cadiz, E. Courtade, C. Robert, G. Wang, Y. Shen, H. Cai, T. Taniguchi, K. Watanabe, H. Carrere, D. Lagarde, M. Manca, T. Amand, P. Renucci, S. Tongay, X. Marie, and B. Urbaszek,

Phys. Rev. X **7**, 021026 (2017).

[45] A. T. Hanbicki, H.-J. Chuang, M. R. Rosenberger, C. S. Hellberg, S. V. Sivaram, K. M. McCreary, I. I. Mazin, and B. T. Jonker, ACS Nano 12, 4719 (2018).

[46] C. Lee, H. Yan, L. E. Brus, T. F. Heinz, J. Hone, and S. Ryu, ACS Nano **4**, 2695 (2010).

[47] H. Li, Q. Zhang, C. C. R. Yap, B. K. Tay, T. H. T. Edwin, A. Olivier, and D. Baillargeat, Adv. Funct. Mater. **22**, 1385 (2012).

[48] L. Du, T. Zhang, M. Liao, G. Liu, S.Wang, R. He, Z. Ye, H. Yu, R. Yang, D. Shi, Y. Yao, and G. Zhang, Phys. Rev. B **97**, 165410 (2018).

[49] W. Zhao, Z. Ghorannevis, K. K. Amara, J. R. Pang, M. Toh, X. Zhang, C. Kloc, P. H. Tan, and G. Eda, Nanoscale **5**, 9677 (2013).

[50] X.-X. Zhang, Y. You, S. Y. F. Zhao, and T. F. Heinz, Phys. Rev. Lett. **115**, 257403 (2015).

[51] M. Molas, C. Faugeras, A. Slobodeniuk, K. Nogajewski, M. Bartos, D. Basko, and M. Potemski, 2D Mater. **4**, 021003 (2017).

[52] G. Wang, C. Robert, M. M. Glazov, F. Cadiz, E. Courtade, T. Amand, D. Lagarde, T. Taniguchi, K. Watanabe, B. Urbaszek, and X. Marie, Phys. Rev. Lett. **119**, 047401 (2017).

[53] J. Serrano, A. Bosak, R. Arenal, M. Krisch, K. Watanabe, T. Taniguchi, H. Kanda, A. Rubio, and L. Wirtz, Phys. Rev. Lett. **98**, 095503 (2007).

[54] I. Hamdi and N. Meskini, Phys. B: **405**, 2785 (2010).

[55] R. Geick, C. Perry, and G. Rupprecht, Phys. Rev. **146**, 543 (1966).

[56] M. Born and K. Huang, *Dynamical theory of crystal lattices* (Oxford University Press, Oxford, 1954).

[57] It should be noted that the activated mode in ref. 37 should be located at 806 cm^{-1} instead of 820 cm^{-1} since 806 cm^{-1} is the center of the activated mode.

[58] L. Zhang and Q. Niu, Phys. Rev. Lett. **115**, 115502 (2015).

[59] H. Zhu, J. Yi, M.-Y. Li, J. Xiao, L. Zhang, C.-W. Yang, R. A. Kaindl, L.-J. Li, Y. Wang, and X. Zhang, Science **359**, 579 (2018).

[60] C. Chen, X. Chen, H. Yu, Y. Shao, Q. Guo, B. Deng, S. Lee, C. Ma, K. Watanabe, T. Taniguchi, J.-G. Park, S. Huang, W. Yao, and F. Xia, ACS Nano **13**, 552 (2019).

[61] L. M. Zhang, G. O. Andreev, Z. Fei, A. S. McLeod, G. Dominguez, M. Thiemens, A. Castro-Neto, D. Basov, and M. M. Fogler, Phys. Rev. B **85**, 075419 (2012).

[62] K. F. Mak, C. Lee, J. Hone, J. Shan, and T. F. Heinz, Phys. Rev. Lett. **105**, 136805 (2010).

[63] A. Splendiani, L. Sun, Y. Zhang, T. Li, J. Kim, C.-Y. Chim, G. Galli, and F. Wang, Nano Lett. **10**, 1271 (2010).

[64] I. Stenger, L. Schue, M. Boukhicha, B. Berini, B. Placais, A. Loiseau, and J. Barjon, 2D Mater. **4**, 031003 (2017).

[65] L. Du, H. Yu, M. Liao, S. Wang, L. Xie, X. Lu, J. Zhu, N. Li, C. Shen, P Chen, R. Yang, D. Shi, and G. Zhang, Appl. Phys. Lett. **111**, 263106 (2017).

[66] K. Liu, L. Zhang, T. Cao, C. Jin, D. Qiu, Q. Zhou, A. Zettl, P. Yang, S. G. Louie, and F. Wang, Nat. Commun. **5**, 4966 (2014).

[67] M. Liao, Z.-W. Wu, L. Du, T. Zhang, Z. Wei, J. Zhu, H. Yu, J. Tang, L. Gu, Y. Xing, R. Yang, D. Shi, Y. Yao, and G. Zhang, Nat. Commun. **9**, 4068 (2018).

[68] J. Kunstmann, F. Mooshammer, P. Nagler, A. Chaves, F Stein, N. Paradiso, G. Plechinger, C. Strunk, C. Schüller, G. Seifert, D. R. Reichman and Tobias Korn, Nat. Phys. **14**, 801 (2018).

[69] G. Eliel, M. V. O. Moutinho, A. C. Gadelha, A. Righi, L. C. Campos, H. B. Ribeiro, P.-W. Chiu, K. Watanabe, T. Taniguchi, P. Puech, M. Paillet, T. Michel, P. Venezuela, and M. A. Pimenta, Nat. Commun. **9**, 1221 (2018).

[70] A. Chernikov, T. C. Berkelbach, H. M. Hill, A. Rigosi, Y. Li, O. B. Aslan, D. R. Reichman, M. S. Hybertsen, and T. F. Heinz, Phys. Rev. Lett. **113**, 076802 (2014).

[71] G. Plechinger, P. Nagler, A. Arora, A. G. del Águila, M. V. Ballottin, T. Frank, P. Steinleitner, M. Gmitra, J. Fabian, P. C. M. Christianen, R. Bratschitsch, C. Schüller, and T. Korn, Nano Lett. **16**, 7899 (2016).

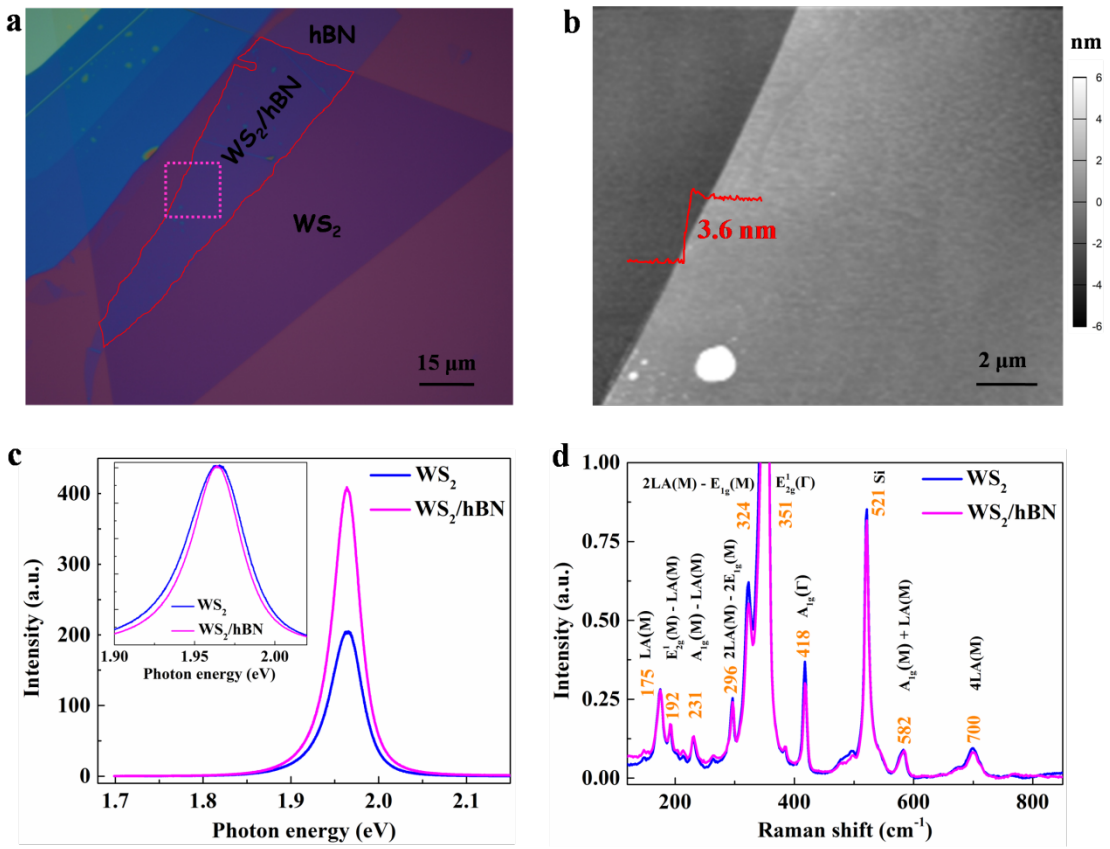

FIG 1. (a) Optical micrograph of a representative WS_2/hBN heterostructures sample. WS_2/hBN heterostructures are highlighted by red lines. (b) Atomic force micrograph taken from the area indicated by dotted square in (a) and the height line scan profile. (c) PL spectra of WS_2 (blue line) and WS_2/hBN heterostructures (magenta line) at 2.33 eV excitation. Inset is the normalized PL spectra around 1.96 eV. (d) Raman spectra of WS_2 (blue line) and WS_2/hBN heterostructures (magenta line) under 2.33 eV excitation.

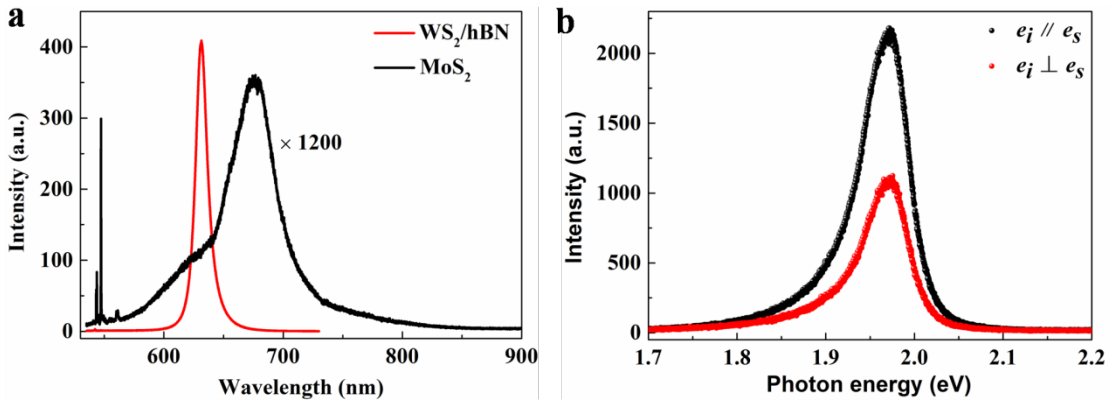

FIG 2. (a) PL spectra of WS_2/hBN heterostructures (red) and monolayer MoS_2 (blue) and under 2.33 eV excitation. (b) Linear-polarization-resolved PL spectra of WS_2/hBN heterostructures at room temperature. Black and red curves present co-polarized configuration (incident light polarization e_i and scattered light polarization e_s are parallel to each) and cross-polarized (incident light polarization and scattered light polarization are perpendicular to each), respectively.

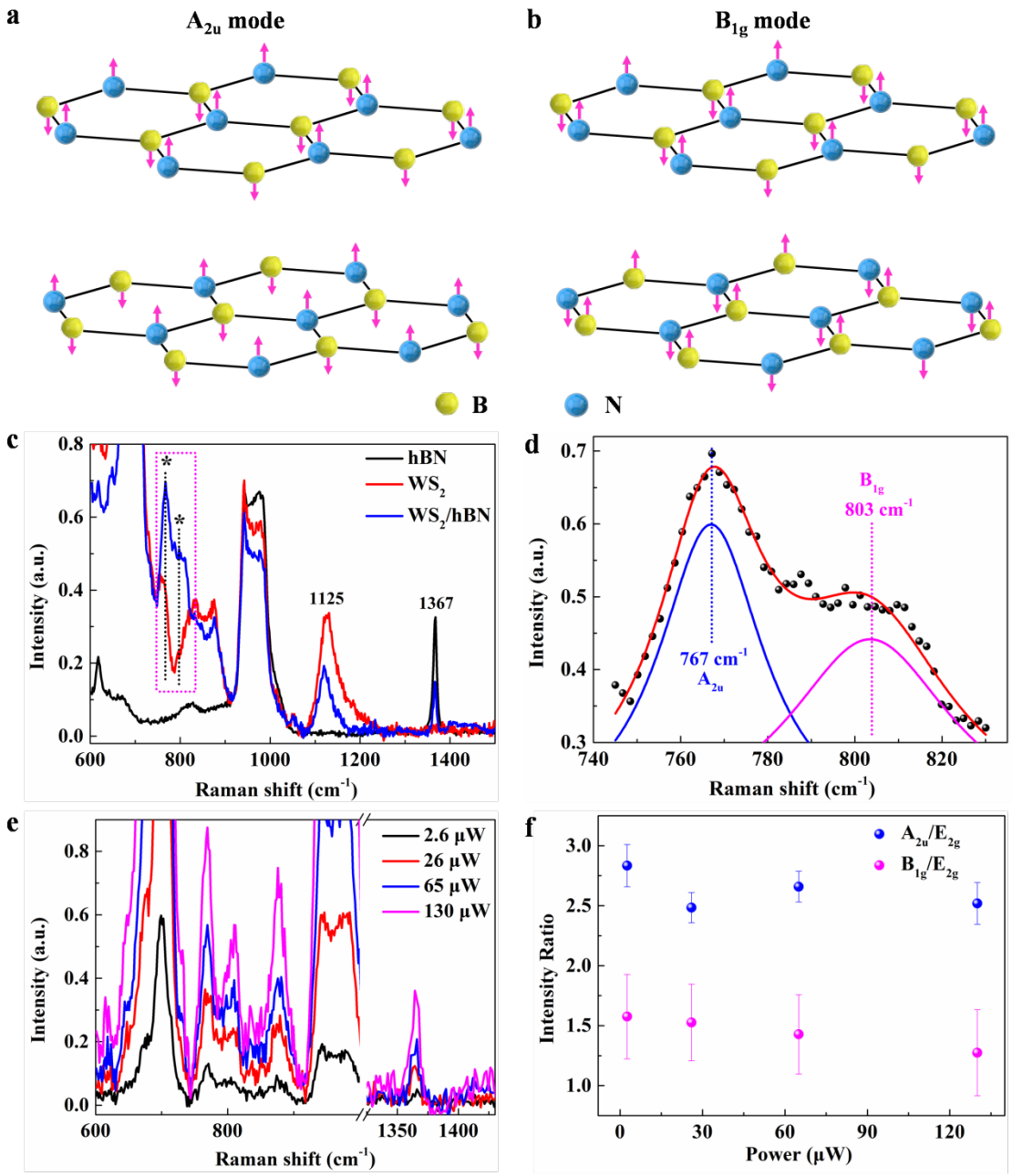

FIG 3. (a) Schematic representation of the atomic motion for infrared active A_{2u} mode. (b) Illustration of the atomic displacements for optically silent B_{1g} mode. (c) Raman spectra of hBN (black), WS_2 (red) and WS_2/hBN heterostructures (blue) with 2.33 eV excitation, on resonance with the B exciton of WS_2. (d) Zoom-in and Lorentzian fitting of the Raman spectrum of WS_2/hBN heterostructures indicated by magenta dotted square in (c). (e) Power-dependent Raman spectra. (f) Raman intensity ratio as a function of power.

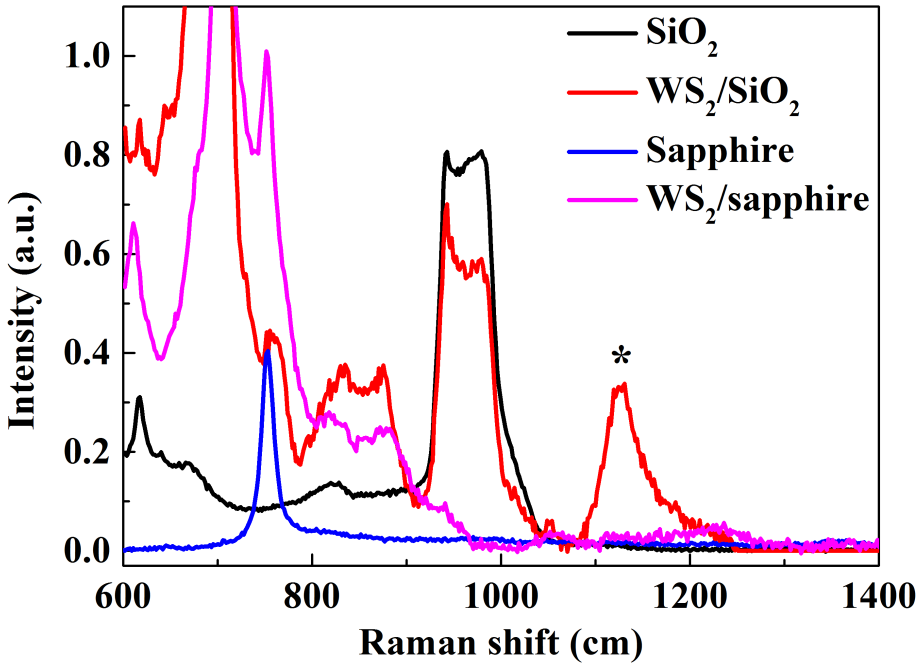

FIG 4. Raman spectra of SiO_2 (black line), WS_2/SiO_2 (red line), sapphire (blue line) and WS_2/sapphire (magenta line) under 2.33 eV excitation.

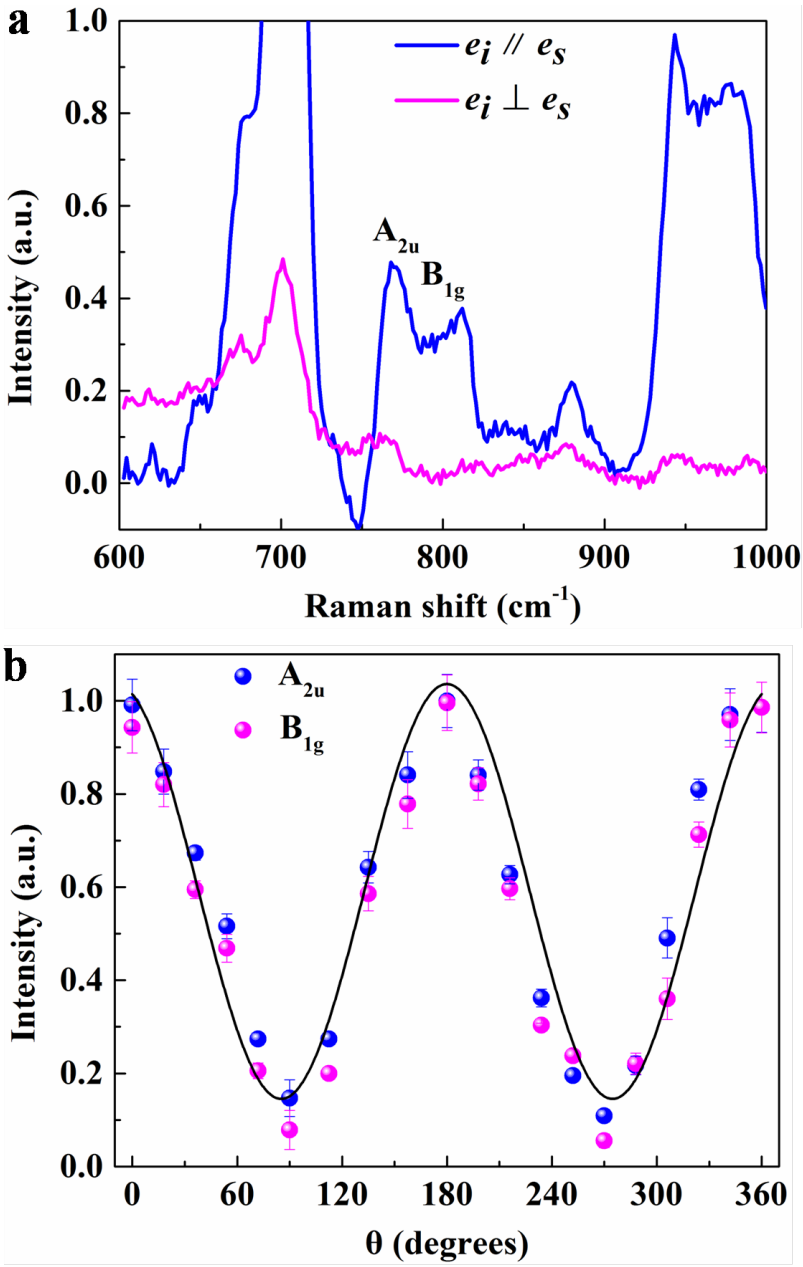

FIG 5. (a) Raman spectra of WS_2/hBN heterostructures obtained in the co-polarized configuration (e_i // e_s) and cross-polarized configuration (e_i ⊥ e_s), where e_i and e_s are the polarization vectors of incident light and scattered photons, respectively. (b) Normalized Raman intensity of A_{2u} and B_{1g} modes as a function of angle θ between e_i and e_s. The black line is the fitting with function of $\cos^2\theta$.

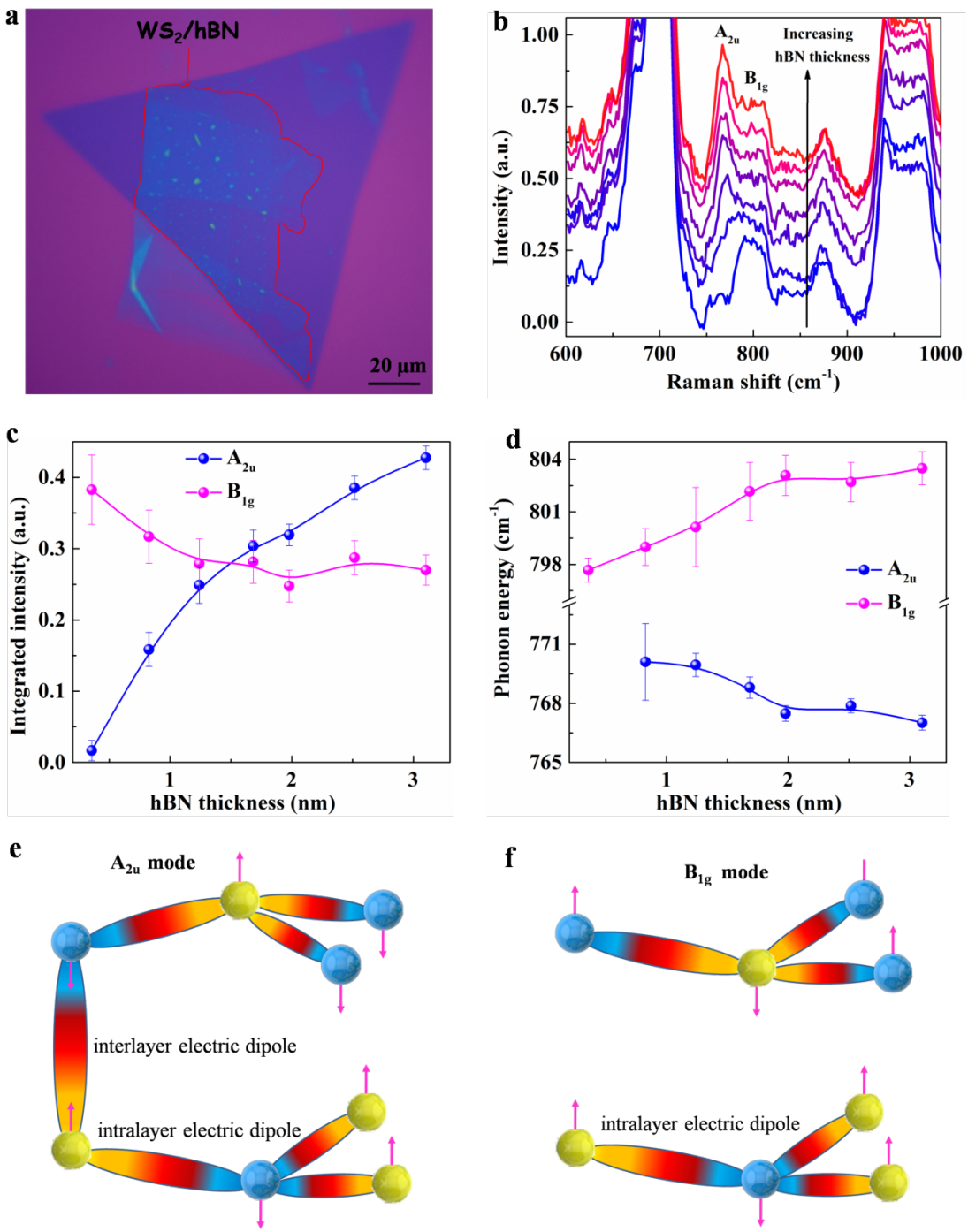

FIG 6. (a) Optical micrograph of a WS_2/hBN heterostructures sample with different thicknesses of hBN. WS_2/hBN heterostructures are highlighted by red lines. (b) Raman spectra of WS_2/hBN heterostructures with distinct hBN thicknesses under 2.33 eV excitation, on resonance with the B exciton of WS_2. (c,d) The Raman intensities (c) and phonon energy (d) of A_{2u} and B_{1g} phonons as a function of hBN thickness. (e,f) Schematic of the electric dipole for A_{2u} (e) and B_{1g} (f) phonons.